Computers & Fluids 38 (2009) 950–964

Contents lists available at ScienceDirect

Computers & Fluids

journal homepage: www.elsevier.com/locate/compfluid

Effect of tube spacing on the vortex shedding characteristics of laminar flow past an inline tube array: A numerical study

Chunlei Liang [c], George Papadakis [b,*], Xiaoyu Luo [a]

[a] Department of Mathematics, University of Glasgow, Glasgow G12 8QW, UK
[b] Department of Mechanical Engineering, King's College London, Strand, London WC2R 2LS, UK
[c] Aeronautics and Astronautics, Stanford University, CA 94305, USA

ARTICLE INFO

Article history:
Received 13 May 2008
Received in revised form 19 October 2008
Accepted 27 October 2008
Available online 14 November 2008

ABSTRACT

The effect of tube spacing on the vortex shedding characteristics and fluctuating forces in an inline cylinder array is studied numerically. The examined Reynolds number is 100 and the flow is laminar. The numerical methodology and the code employed to solve the Navier–Stokes and continuity equations in an unstructured finite volume grid are validated for the case of flow past two tandem cylinders at four spacings. Computations are then performed for a six-row inline tube bank for eight pitch-to-diameter ratios, s, ranging from 2.1 to 4. At the smallest spacing examined ($s = 2.1$) there are five stagnant and symmetric recirculation zones and weak vortex shedding activity occurs only behind the last cylinder. As s increases, the symmetry of the recirculation zones breaks leading to vortex shedding and this process progressively moves upstream, so that for $s = 4$ there is clear shedding from every row. For any given spacing, the shedding frequency behind each cylinder is the same. A critical spacing range between 3.0 and 3.6 is identified at which the mean drag as well as the rms lift and drag coefficients for the last three cylinders attain maximum values. Further increase to $s = 4$ leads to significant decrease in the force statistics and increase in the Strouhal number. It was found that at the critical spacing there is 180° phase difference in the shedding cycle between successive cylinders and the vortices travel a distance twice the tube spacing within one period of shedding.

© 2008 Elsevier Ltd. All rights reserved.

1. Introduction

Flow around a group of cylinders is very often encountered in engineering practice. For example, tube banks are widely employed in process industries and especially in the power generation and oil industry (heat exchangers in boilers or nuclear reactors, offshore risers, etc.). Other applications include flow around hollow fiber arrays with many applications in absorption, extraction and ultra-filtration [15] or paper machine forming fabrics [6]. In the latter examples the flow is laminar with Reynolds number in the order of 150–200.

The flow across a group of cylinders is very rich in fluid dynamics phenomena. Even for the flow around two cylinders, Sumner et al. [29] identified nine different flow patterns depending on the angle of incidence and spacing between the tubes. Complex flow dynamic phenomena such as reattachment of shear layers, induced separation, vortex synchronisation and impingement or vortex pairing, splitting and enveloping were observed. There are numerous other papers, experimental and computational, on the flow around two cylinders: [1,9,19,22,30,33] to cite just a few. In the paper of Sumner et al. [30] there is a table that lists 23 experimental studies. However, much fewer studies have been carried out for more cylinders; Lam and Cheung [12] and Igarashi and Suzuki [7] investigated the flow around three cylinders while Lam et al. [13,14] examined four cylinders. Recently simulations of non-Newtonian power-law fluids at low Reynolds numbers over a pair of cylinders in tandem have appeared [23].

On the other hand, a lot of experimental and numerical work has been carried out in flows around tube bundles that consist of a large number of tubes. There are many array configurations, such as inline [11,34,35], staggered symmetric [2,3], rotated square [25,28,32], normal triangle [20,24], parallel triangle [25,36], etc.

One of the first attempts for a systematic analysis of shedding phenomena that affect tube vibration was that of Owen [21]. He found that the dominant frequency of vibration in a bank of tubes, for which the non-dimensional transverse spacing lies between 1.65 and 5, is equal to the interstitial gas velocity divided by twice the distance between successive rows in the streamwise direction. Later Weaver et al. [31] found that the Strouhal number evaluated using this hypothesis matches quite well the experimental data for square inline arrays with pitch ratio from 1.2 to 3.0. Ziada and Oengören [34,35] have studied the vortex shedding characteristics in inline arrays with small, intermediate and large spacings. They found that the vorticity shedding phenomenon in the small (less than 1.5) and intermediate (between 1.75 and 2.7) spacings is gen-

* Corresponding author. Tel.: +44 (0) 20 7848 2049.
E-mail address: george.papadakis@kcl.ac.uk (G. Papadakis).

0045-7930/$ - see front matter © 2008 Elsevier Ltd. All rights reserved.
doi:10.1016/j.compfluid.2008.10.005

erated by the symmetric instability of the jet issuing from the flow lanes between adjacent tube rows. They call this the "global instability mode". For bigger spacings (larger than 2.7) vortex shedding can occur at either the "global jet mode" or the "local wake mode". In the latter mode, the shedding in each row becomes independent from the shedding at adjacent rows, as would be expected for arrays with large transverse spacings.

For many practical applications, especially in the power generation industry from solid fuels (coal, lignite, etc.), the heat exchangers above the combustion zone have wide spacings in the cross-stream direction in order to avoid blockage of the gas lanes due to fouling from ash deposits on the tube walls. Konstantinidis et al. [11] studied experimentally the flow in such an inline tube bundle with spacings 2.1×3.6 in the streamwise and transverse directions, respectively. Flow visualisation showed that there is 180° phase difference between successive rows. For example, when the shear layer from one cylinder folded toward one side, the shear layer from the downstream cylinder folded on the opposite side. They mention that this synchronisation of vortex shedding was the reason for a well defined frequency in the bundle.

To the best of our knowledge this synchronisation of vortex shedding in multiple cylinder arrays, and most importantly its implication on the mean and rms forces acting on each cylinder, has not been studied so far. Previous LES simulations of inline tube arrays by Hassan and Ibrahim [5] did not report this phenomenon possibly because the square arrays studied were closely packed (spacings 1.4 and 1.5). The aim of this paper is therefore to fill this gap. It is clear that more than two cylinders are needed to capture this phenomenon and in the present study six cylinders in tandem are examined. The effect of spacing on the vortex shedding characteristics and the values of the mean/rms of lift and drag coefficients is examined in detail. The results are directly transferable to inline tube arrays with large spacings in the cross-stream direction.

The paper is organised as follows. Section 2 provides details on the numerical approach and solution method employed. In order to validate the methodology and computer code employed, Section 3 presents comparison with the results of Sharman et al. [27] for the laminar flow past two cylinders in tandem. Results for the inline array consisting of six rows are presented and discussed at Section 4. Finally, Section 5 summarises the main findings of this work.

2. Numerical approach and solution method

The incompressible Navier–Stokes equations are written in tensorial Cartesian form as:

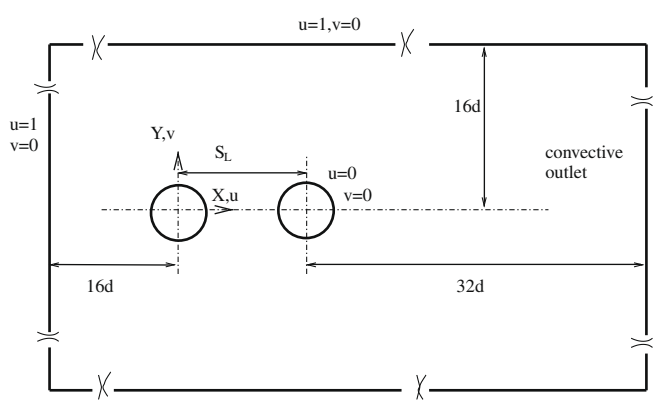

Fig. 1. Computational domain and boundary conditions for two cylinders in-tandem.

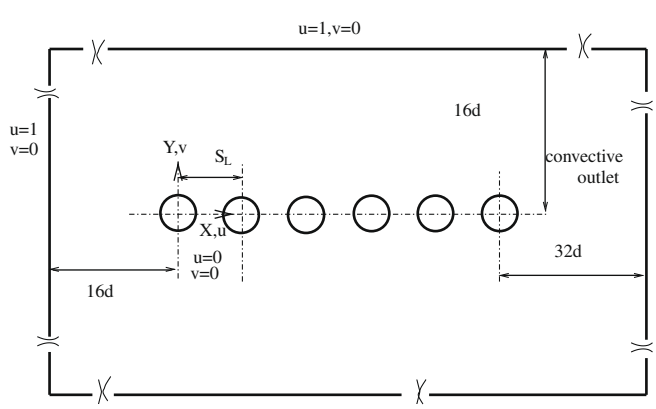

Fig. 2. Computational domain and boundary conditions for a six-row inline tube bank.

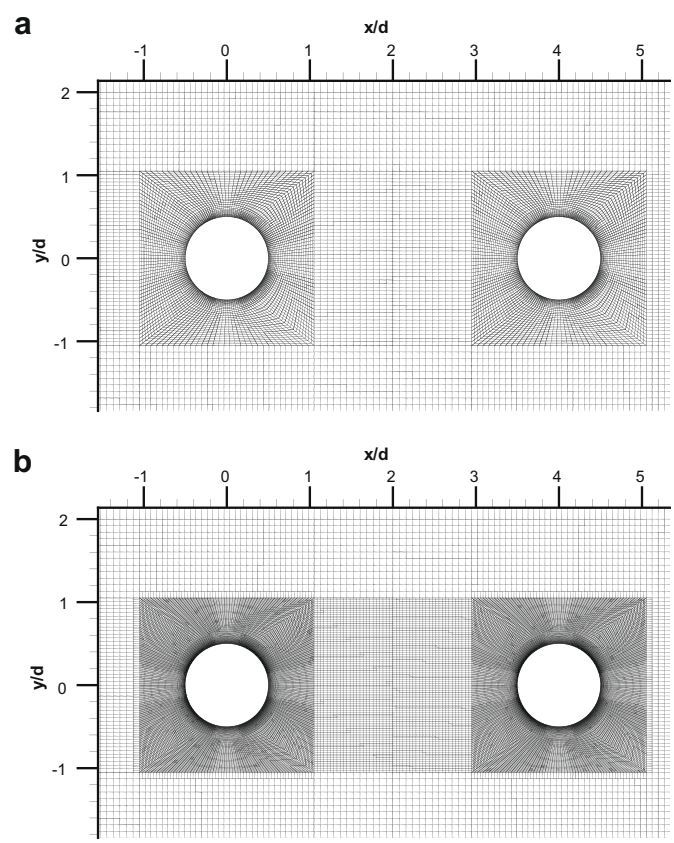

Fig. 3. Zoomed-in view of the computational mesh for the 2-cylinder arrangement with $s = 4.0$: (a) coarser mesh and (b) finer mesh.

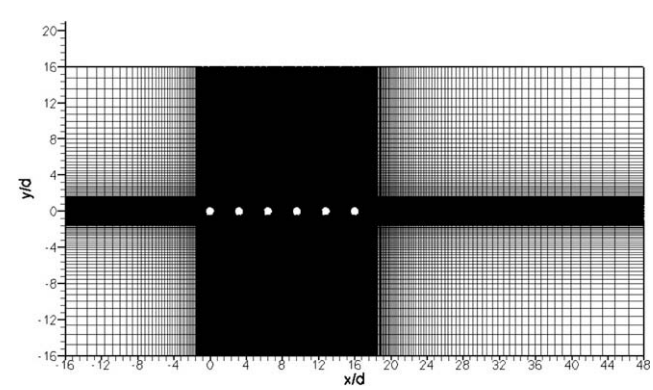

Fig. 4. The computational mesh for the inline tube bank with $s = 3.2$.

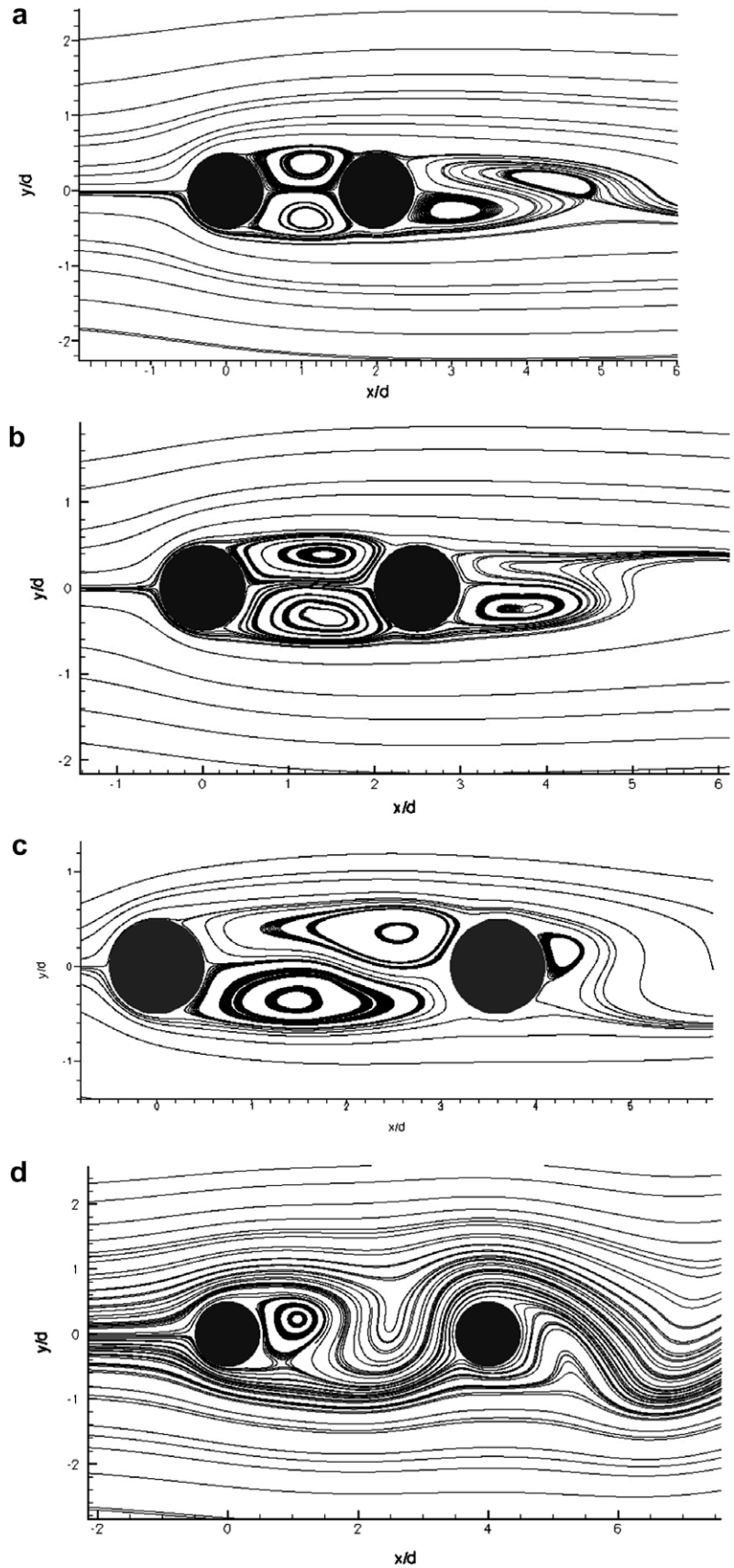

Fig. 5. Instantaneous streamlines for two cylinders in tandem with: (a) $s = 2$, (b) $s = 2.5$, (c) $s = 3.6$, and (d) $s = 4.0$.

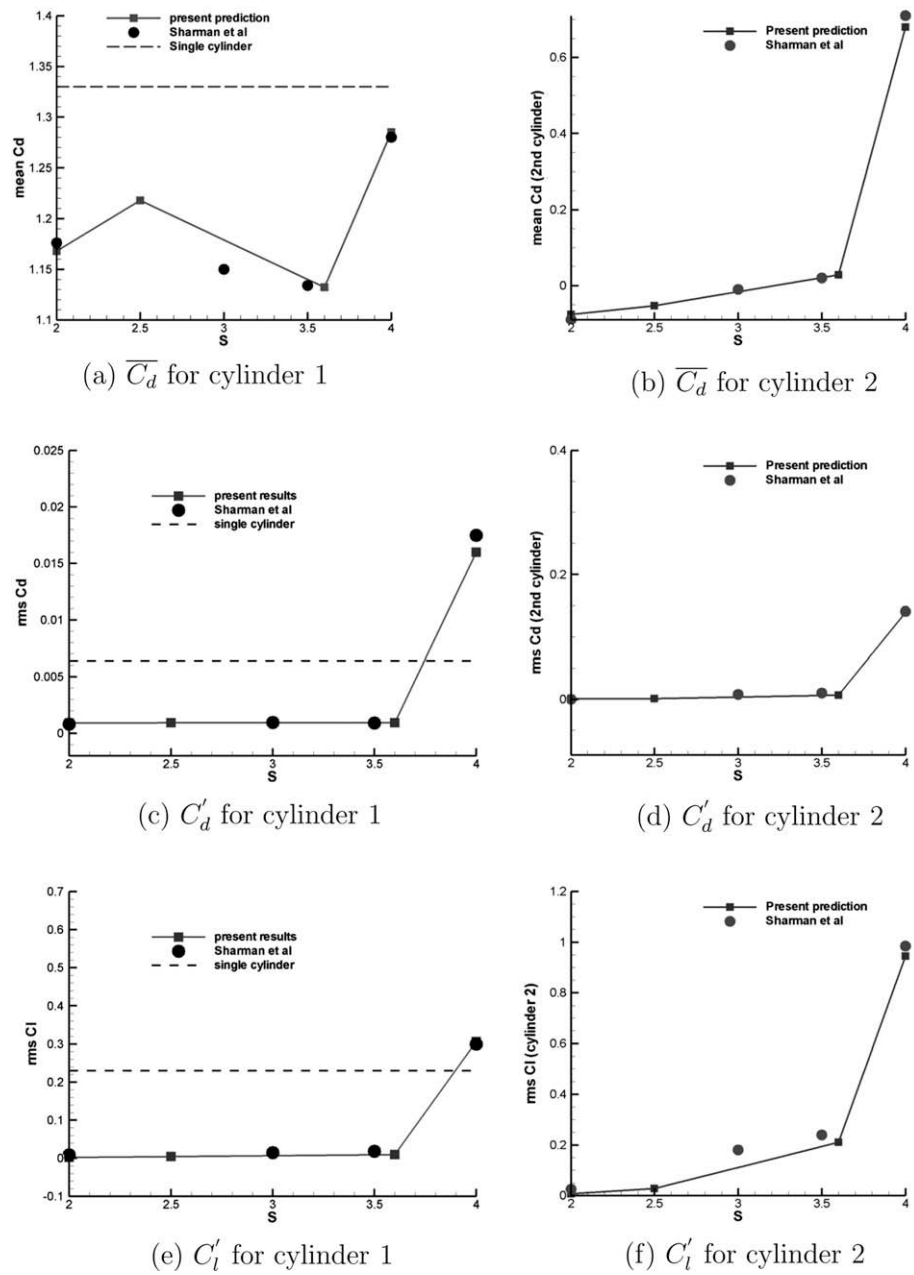

Fig. 6. Statistical forces for two-in-tandem cylinders at different spacings; comparison with the data of Sharman et al. [27] and the values for a single cylinder.

$$\frac{\partial u_i}{\partial x_i} = 0, \tag{1}$$

$$\frac{\partial u_i}{\partial t} + \frac{\partial u_i u_j}{\partial x_j} = -\frac{1}{\rho}\frac{\partial P}{\partial x_i} + \nu \frac{\partial^2 u_i}{\partial x_j \partial x_j}, \tag{2}$$

where the indices ($i,j = 1,2,3$) represent the three directions in a Cartesian coordinate system, u_i is the flow velocity in the ith direction, P is the pressure, ρ the fluid density and ν the kinematic viscocity.

The finite volume method applied on an unstructured, collocated grid arrangement is employed to discretize the above equations. The developed in-house code has been used in the past to simulate successfully bluff body flows, such as the 3D pulsating flow over a single circular cylinder at Reynolds number 2580 [17] and the flow in a staggered tube array [16] using the LES technique. All spatial terms in the momentum equations are discretized using the second order central differencing scheme (CDS) while the second order accurate Crank–Nicolson method is employed to advance them in time. The pressure term is treated fully implicitly, i.e. evaluated at the new time instant. The PISO scheme Issa [8] is used to deal with the pressure-velocity coupling between the momentum and the continuity equations. In order to avoid the check-board pressure field, the velocity interpolation method at the cell faces proposed by Rhie and Chow [26] is employed.

A convective boundary condition $\frac{\partial \phi}{\partial t} + U_{conv}\frac{\partial \phi}{\partial x} = 0$ is used for the exit boundary, where U_{conv} is the velocity normal to the outlet boundary and ϕ is any physical variable that is convected out of the domain. No-slip conditions are used for the cylinder walls. The normal derivative for the pressure correction is set to zero at all boundaries.

All simulations are two dimensional because the Reynolds number (defined as $Re = \frac{U_\infty d}{\nu}$) is equal to 100, i.e. not sufficiently large to excite three dimensional effects. Therefore, in the spanwise direction, only one computational cell is used and symmetry boundary conditions are applied. The simulations start with a zero velocity and pressure field, the flow is allowed to develop for

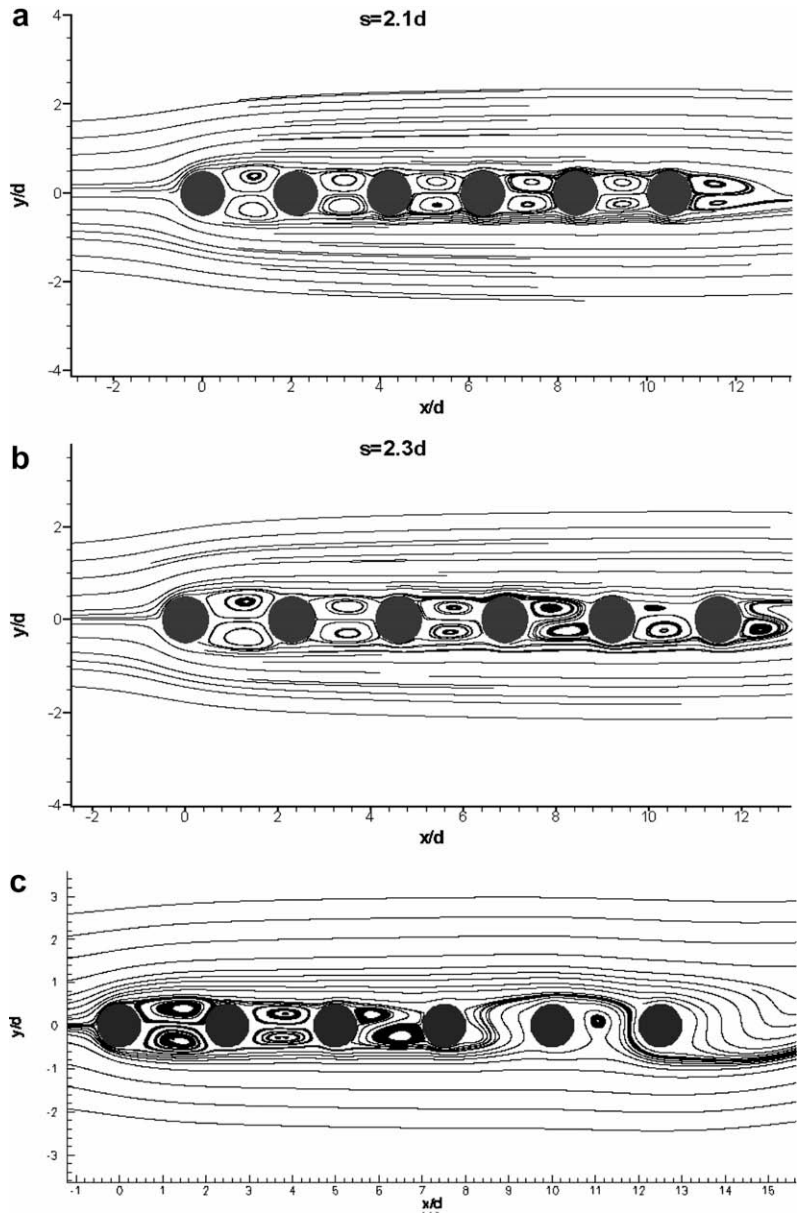

Fig. 7. Instantaneous streamlines past the inline tube bank with: (a) $s = 2.1$, (b) $s = 2.3$, and (c) $s = 2.5$.

around 20 shedding periods and then statistics are collected for more than 10 cycles.

Fig. 1 shows the computational domain for the two cylinders in-tandem arrangement used for validation purposes and Fig. 2 the domain for the six row inline array. The non-dimensional spacing s is defined as $s = S_L/d$, where S_L is shown in Fig. 1 and d is the diameter of the cylinder. For all cases examined the inlet boundary is located 16d upstream of the first cylinder and the exit boundary 32d downstream from the center of the last cylinder. The upper and lower boundaries are placed at 16d away from the row of cylinders, giving a blockage ratio 3.1%.

For the two-cylinder case, four spacings were examined (2, 2.5, 3.6 and 4). Grid independence calculations were performed for the largest spacing $s = 4$ with two meshes consisting of 29,808 and 70,064 cells. A zoomed-in view of the coarser mesh is shown in Fig. 3(a). Blocks with dimensions about $[2D \times 2D]$ around each cylinder were meshed with O-type grids and orthogonal cells filled the rest of the domain. Along the periphery of each cylinder 160 cells were uniformly distributed. This is higher even compared to the number of cells used along the surface in the finest mesh of [27], which was equal to 120. A constant expansion factor 1.03 was used for the cell spacings in the radial direction away from the cylinder wall. The smallest cell thickness in the radial direction was $\Delta r_{min}/d = 4 \times 10^{-3}$. This is comparable to the value 1.25×10^{-3} of the finest mesh used by [4] for LES (with no-slip boundary conditions) around a single cylinder at a much higher Reynolds number (3900). The cells in the gap between two successive cylinders have normally the largest size, about 0.05d. The finer mesh with 70,064 cells was produced by doubling the number of control volumes in each direction in the blocks surrounding the cylinders and in the gap area (Fig. 3(b)). As will be shown in the next section, there are small differences in the results obtained from these two meshes.

For the six-tube arrangement, the mesh was again constructed by connecting together individual blocks around each cylinder. The level of resolution for each block corresponds to Fig. 3(a). The total number of cells varied between 72,230 and 179,604

Table 1
Strouhal number behind each cylinder of the inline tube bank.

Ratio s	Strouhal numbers for vortex shedding after each cylinder					
	Cylinder 1	Cylinder 2	Cylinder 3	Cylinder 4	Cylinder 5	Cylinder 6
2.1	–	–	–	–	–	0.08
2.3	–	–	–	0.0875	0.0875	0.0875
2.5	–	–	0.0918	0.0918	0.0918	0.0918
2.8	–	0.1	0.1	0.1	0.1	0.1
3	0.1001	0.1001	0.1001	0.1001	0.1001	0.1001
3.2	0.104	0.104	0.104	0.104	0.104	0.104
3.6	0.109	0.109	0.109	0.109	0.109	0.109
4	0.1502	0.1502	0.1502	0.1502	0.1502	0.1502

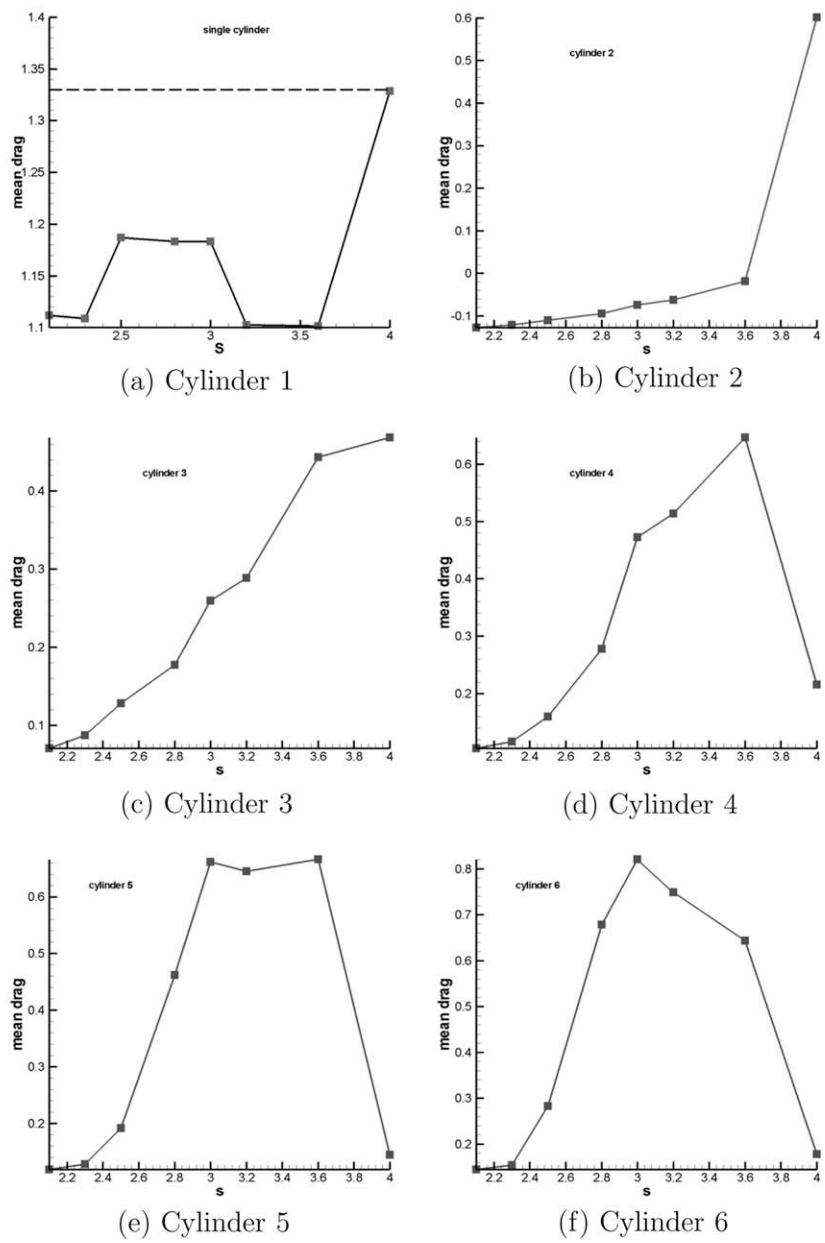

Fig. 8. Variation of $\overline{C_d}$ against s for each cylinder.

depending on the spacing. Fig. 4 shows the computational grid for for $s = 3.2$ that contains 120,836 cells.

Around 16 iterations are required for convergence of the equations within each time step to within a prescribed tolerance of 10^{-3} for the normalised residuals. The simulations were carried out on a DELL Workstation 490, with Dual processor Xeon 3.06 GHz and 4 GB of RAM. The calculations were serial and one case takes around 75 h in total (including the

time to develop a steady and repeatable vortex shedding pattern).

3. Flow around two cylinders in tandem (validation study)

The unsteady flow past two cylinders in tandem was computed first. This is an excellent case for the validation of the employed methodology and computer code. It serves also as an "introduction" to the flow behind more cylinders. Computations were carried out for four values of s (2, 2.5, 3.6 and 4) as already mentioned.

Snapshots of instantaneous streamlines are shown in Fig. 5. The simulations show that for $s = 2$ there is no distinct vortex shedding in the gap between the two cylinders and a stagnant symmetric vortex pair develops instead. The flow behind the second cylinder is found to be bimodal; the numerical simulation predicts a pair of symmetric vortices but when an artificial asymmetric perturbation is imposed for a short interval, vortices start to shed off as evidenced in Fig. 5(a). The Strouhal number predicted is 0.122. For $s = 2.5$ the vortices in the gap are still symmetric and a small artificial perturbation was again imposed for a small time interval in order to trigger vortex shedding behind the downstream cylinder (Fig. 5(b)). For $s = 3.6$, asymmetries develop in the two gap vortices (Fig. 5(c)) while finally for $s = 4$ there is clear shedding in the gap (Fig. 5(d)).

The variation of the force statistics for both cylinders with s is shown in Fig. 6. The mean drag coefficient of the first cylinder, $\overline{C_{d,1}}$, is smaller than the value for a single cylinder at Re = 100 (equal to 1.33 and shown with a dotted line in Fig. 6(a)) but it approaches this value for $s = 4$. For small values of s, the mean drag coefficient for cylinder 2, $\overline{C_{d,2}}$, is negative, i.e. the cylinder is pushed upstream. The presence of negative drag coefficients is well known and has been reported by Zdravkovich [33] among others. The smallest value is obtained for $s = 2$ and then $\overline{C_{d,2}}$ increases gradually until 3.6 and then very rapidly between 3.6 and 4.0. The value at $s = 4$ is about one half of the value for a single cylinder.

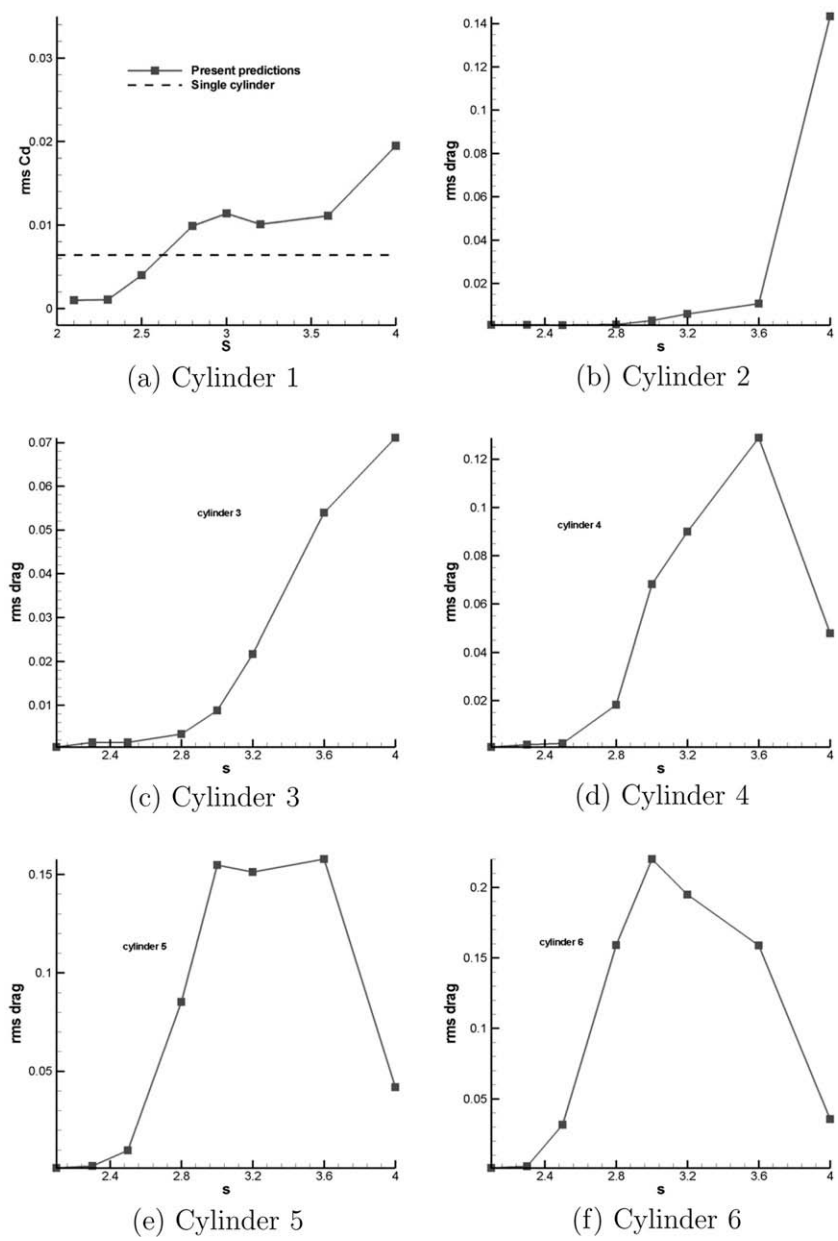

Fig. 9. Variation of C'_d against s for each cylinder.

For $s \leqslant 3.6$, the rms values of drag and lift coefficients for the first cylinder, $C'_{d,1}$ and $C'_{l,1}$, respectively, are very small because of the aforementioned stagnant vortices in the gap region. The values increase rapidly between $s = 3.6$ and $s = 4$. Although there is clear vortex shedding behind the second cylinder for both $s = 2$ and $s = 2.5$, it is very weak and so $C'_{d,2}$ and $C'_{l,2}$ are also close to zero. Again the values increase rapidly from $s = 3.6$ to 4. The larger values of all force statistics at $s = 4$ are due to the clear shedding activity in the gap as shown in Fig. 5(d).

The effect of mesh on the results was examined for $s = 4$. There were small differences; for example the mean C_d coefficients for cylinders 1/2 were 1.30/0.68 and 1.28/0.71 for the 29,808-cell mesh and 70,064-cell mesh, respectively. The values for the rms C_l were 0.28/0.95 and 0.30/0.99 for the two meshes, respectively. The Strouhal number was the same behind each cylinder and equal to 0.150 (coarser mesh) and 0.148 (finer mesh).

In Fig. 6 the results with the fine mesh are shown. For all examined spacings there is generally good quantitative agreement between the present results and those of Sharman et al. [27]. The small differences are mainly attributed to the fact that the examined spacings were not identical. For example, the aforementioned authors have studied $s = 3$, which was not examined in the present paper, and this can explain the small deviation in Fig. 6(a). Another source is the inevitable error from reading the data from the graphs of the paper of Sharman et al. [27].

In summary, the study of the laminar flow past two cylinders in-tandem demonstrates that there is vortex shedding behind the downstream cylinder for all examined spacings. In the gap between two cylinders, there are two symmetric stagnant vortices for $s = 2$ and 2.5. For $s = 3.6$ the two vortices become asymmetric and unstable and vibrate with a relatively small amplitude. There is clear vortex shedding in the gap for $s = 4$ leading to large increases in the rms values of the forces.

4. Flow past an in-line tube bunk

Attention is now turned to the in-line tube bunk that consists of six cylinders.

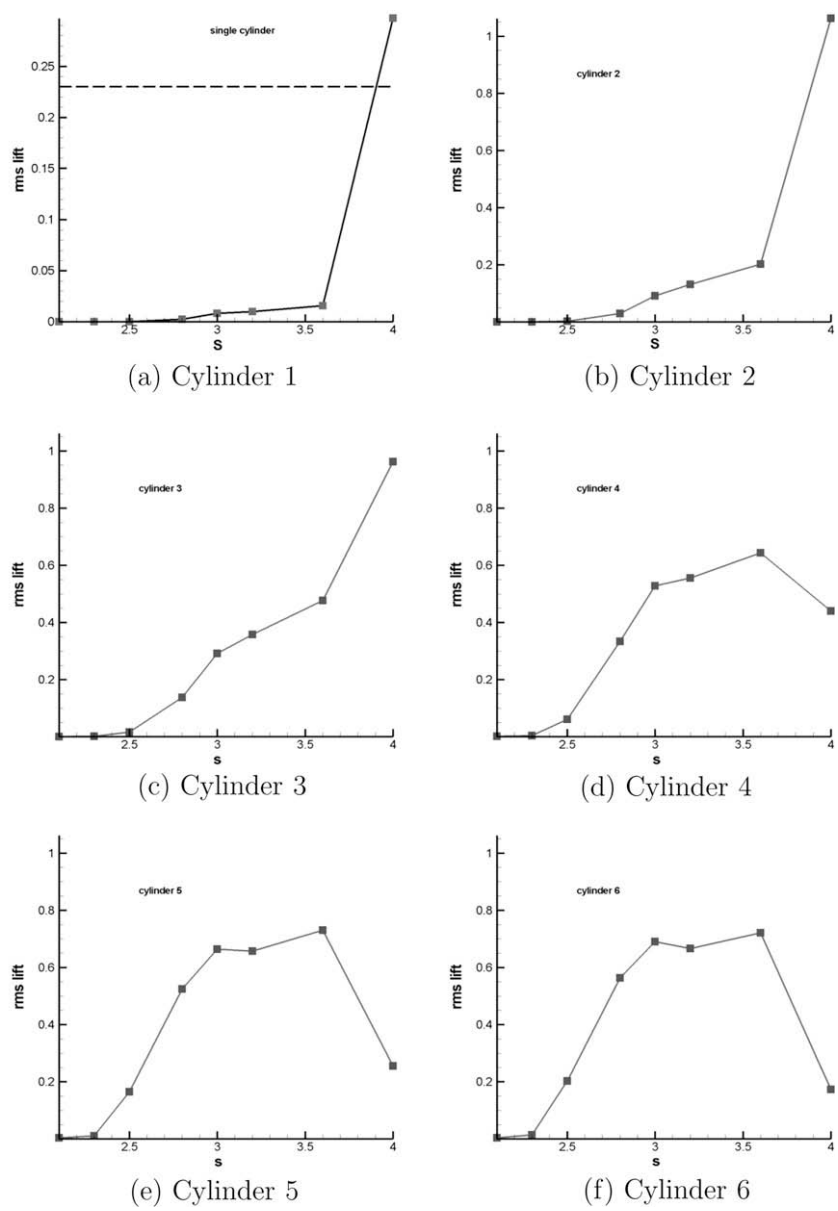

Fig. 10. Variation of C'_l against s for each cylinder.

4.1. Development of vortex shedding and force statistics

The instantaneous flow field for the six-cylinder array is affected enormously by the tube spacing. Fig. 7 shows instantaneous streamline patterns for $s = 2.1$, 2.3 and 2.5. For the smallest value $s = 2.1$, there are five symmetric recirculation zones while the flow behind the sixth cylinder exhibits a weak vortex shedding with Strouhal number 0.08. For $s = 2.3$ there are still three stagnant symmetric vortex formation zones but a stronger asymmetry develops in the last three cylinders as can be seen in Fig. 7(b). For $s = 2.5$ there are two nearly symmetric stagnant vortices formed in the first two gaps. In the gap between third and fourth cylinders, two vortices still co-exist as shown in Fig. 7(c), but the strong asymmetry has developed to distinct vortex shedding (unique Strouhal number 0.0918). From these patterns it can be seen clearly that asymmetries develop in the recirculation zones, starting from the downstream cylinders and, as s increases, they propagate upstream leading to vortex shedding activity from more and more rows. This behaviour is very similar to that observed previously in the two-cylinder arrangement. Table 1 summarises the Strouhal numbers for all the examined arrangements. The frequency is the same for all cylinders shedding vortices, giving a unique Strouhal number for every arrangement.

Fig. 8 shows the variation of the mean drag coefficients for all cylinders against spacing, s. Eight values of s were examined 2.1, 2.3, 2.5, 2.8, 3, 3.2, 3.6 and 4. It is clear that the cylinder spacing has a large impact on the drag values. For all cylinders the mean drag coefficient, $\overline{C_d}$, is smaller than the value for a single cylinder. For the first two cylinders in particular the variation of $\overline{C_d}$ with s is very similar to the previously examined 2-cylinder case. The mean

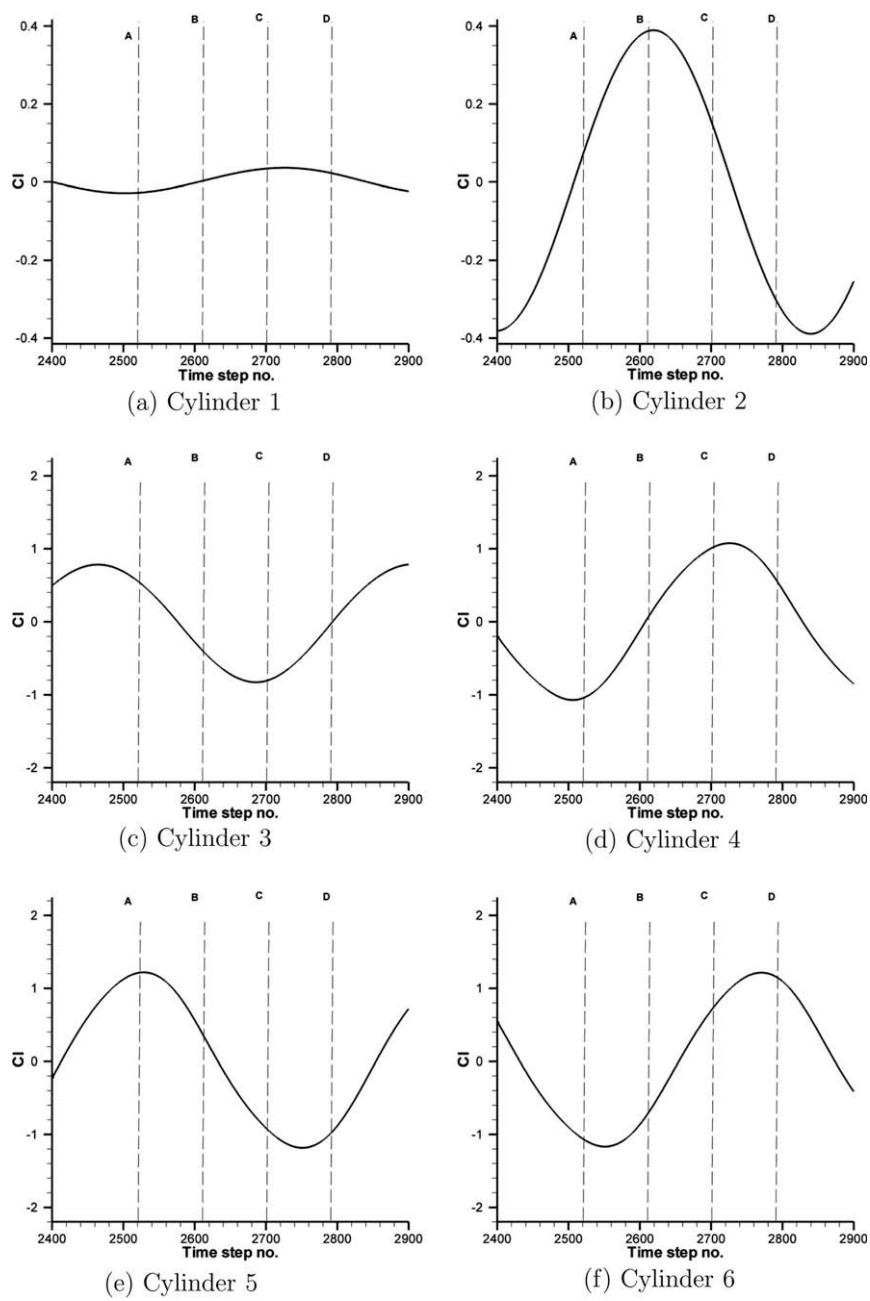

Fig. 11. Variation of the instantaneous lift coefficient with time and definition of phases A–D ($s = 3.6$).

drag coefficient for the third cylinder $\overline{C_{d,3}}$ is always positive and increases almost linearly with s as shown in Fig. 8(c). For the last three cylinders, the variation of $\overline{C_d}$ with s shows many similarities, which indicates that after the third cylinder a periodic pattern starts to develop. The values are positive, increase up to a value 0.65–0.8, remain at high levels in the spacing regime $s = 3.0$–3.6 and then drop suddenly.

Fig. 9 shows rms drag coefficients for all six cylinders. There is a smooth increasing trend for the first cylinder, $C'_{d,1}$, and the values are of the same order to the value of the single cylinder. The level of rms drag coefficient for cylinder 2 increases suddenly between $s = 3.6$ and 4 but cylinder 3 has a more smooth increasing trend. The last three cylinders show again a similar pattern: C'_d increases, reaches high values (0.12–0.2) compared to a single cylinder in the region $s = 3.0$–3.6 and then decreases sharply at $s = 4$.

Fig. 10 shows the rms lift coefficients for all six cylinders. The trends for the first two cylinders are similar to the validation case. For the other four cylinders we can see again the same pattern as for the other two force statistics: smooth increase for cylinder 3 and increase, plateau, decrease for cylinders 4–6. The maximum values of C'_l attained (0.6–0.7) are almost three times larger compared to a single cylinder.

Obviously non-zero values of C'_l, C'_d are due to the unsteadiness of the flow. The small values of these coefficients for small spacings

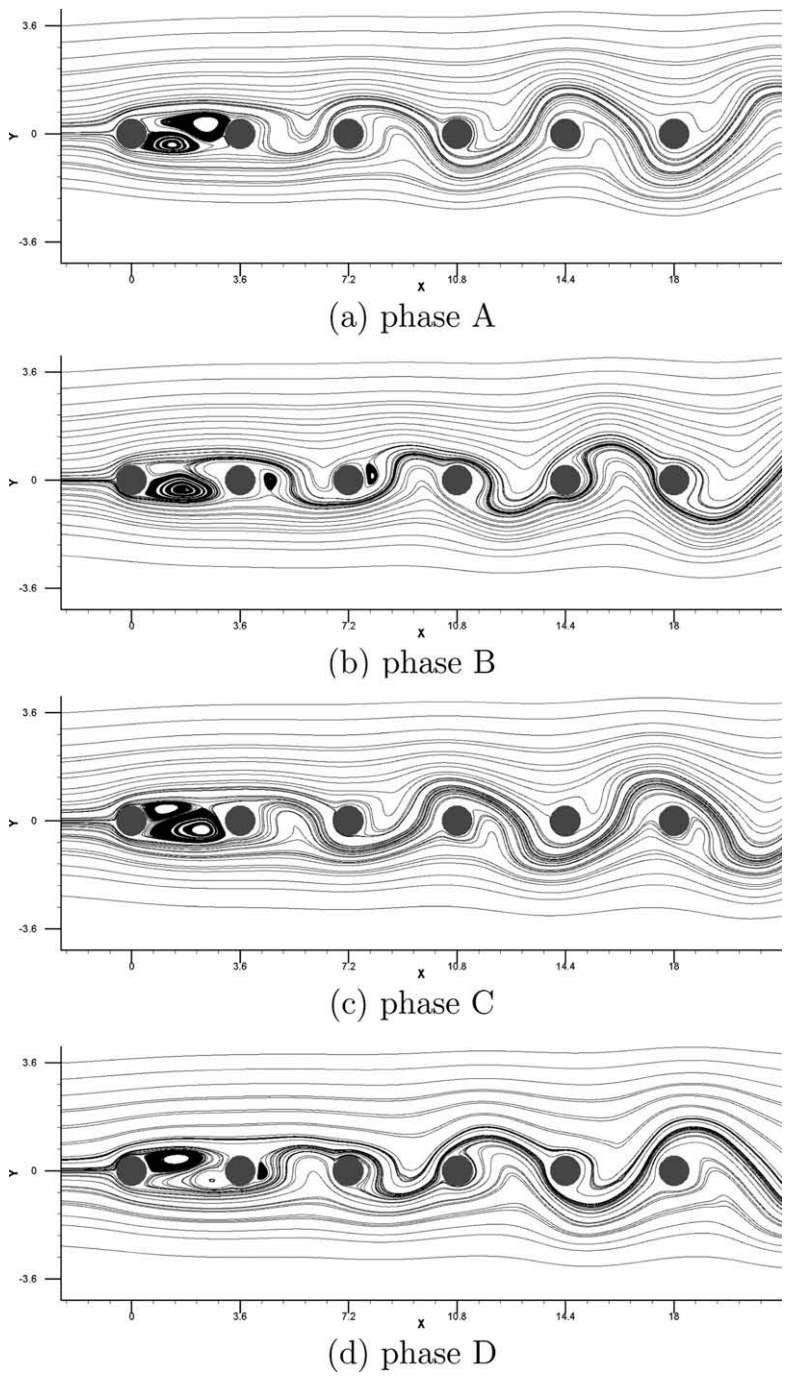

Fig. 12. Streamlines at phases A–D ($s = 3.6$).

can be explained by the weak vortex shedding activity behind the rows as evidenced earlier in Fig. 7. More interesting is the maximisation of the rms forces in the region $s = 3.0$–3.6 and then the sudden drop for $s = 4$. Analysis of the instantaneous flow patterns can shed light into the dynamics of the flow and can help to explain the observed behaviour. This is examined in the next section.

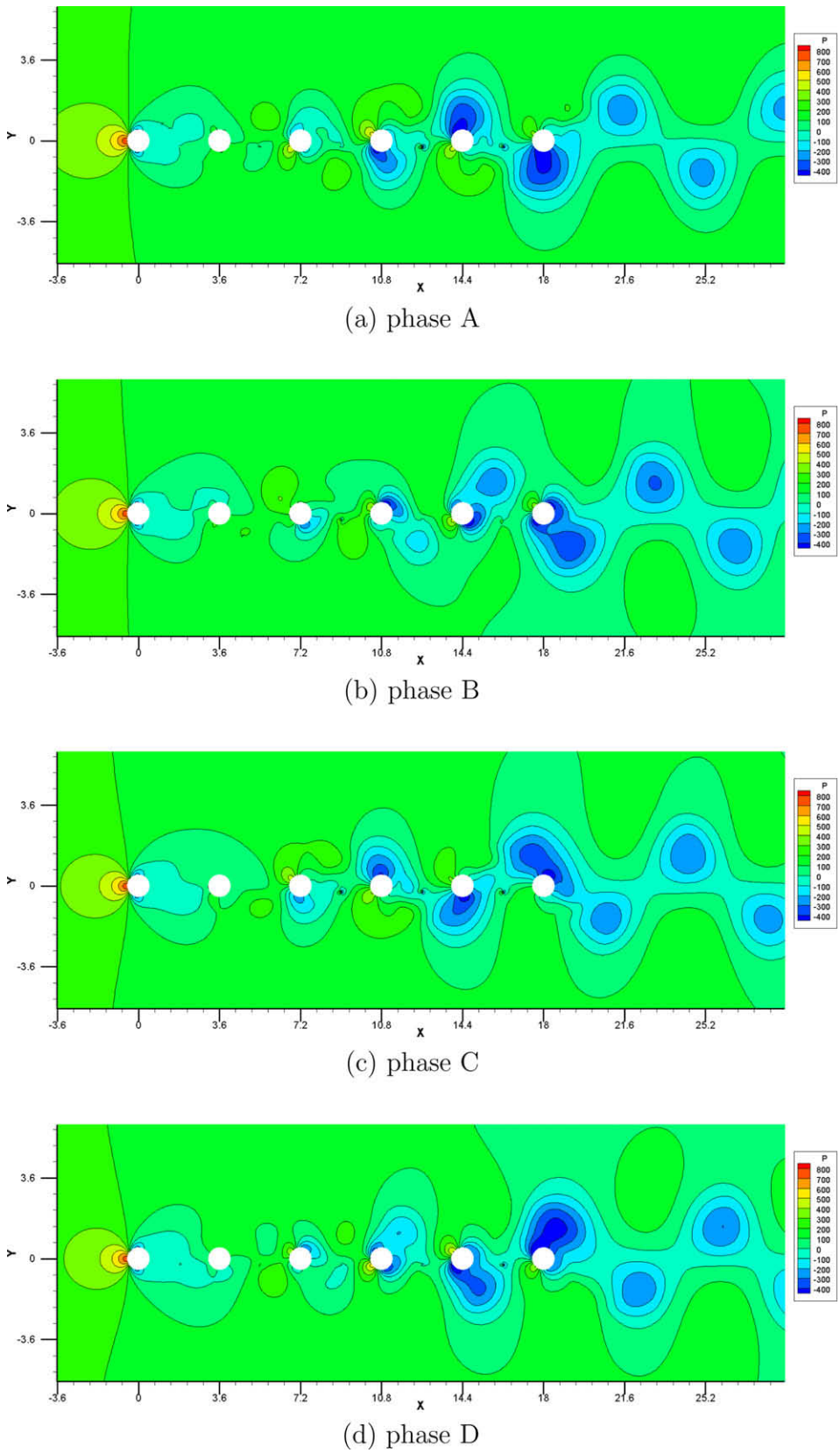

Fig. 13. Pressure contours at phases A–D ($s = 3.6$).

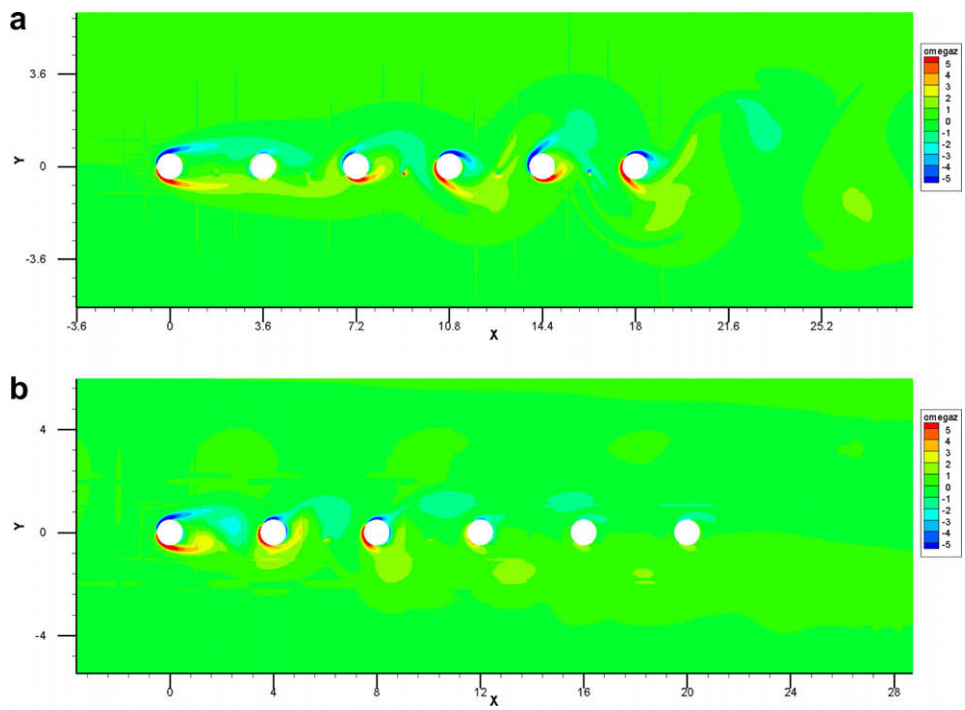

Fig. 14. Vorticity contours (a) $s = 3.6$ (at phase B) and (b) $s = 4$ (at phase B).

4.2. Analysis of the instantaneous flow field for s = 3.6 and 4

In this section a comprehensive analysis of the instantaneous streamlines, pressure and vorticity patterns will be carried out for the two spacings 3.6 and 4.0. The patterns will be correlated with the instantaneous values of the lift coefficient for all cylinders in order to provide a more comprehensive picture of the flow.

Fig. 11 shows the variation of the instantaneous lift coefficients for a vortex shedding period for $s = 3.6$. The Strouhal number is the same for all cylinders in the bank and equal to 0.109. In the last three cylinders, for which as we have seen a repeatable pattern tends to be established, the lift variation indicates a strong phase difference (almost 180°) in the vortex shedding between adjacent rows. However, between the first two cylinders the phase difference is much smaller and increases rapidly between the second and third cylinder.

Four time instants, denoted with the letters A–D, are marked in this figure and snapshots of streamlines at those instants are shown in the following Fig. 12. In the gap between the cylinders 1 and 2, two non-symmetric, vibrating, recirculation zones are present and this can explain the low C_l values in Fig. 11(a). Let us examine in more detail the flow behind the last three cylinders. It can be clearly seen that the same fluid stream passes alternatively from the top and the bottom of successive cylinders. The stream is deflected by the vortex shedding activity behind each cylinder leading to wide oscillations in the frontal angle of impingement. This in turn leads to large variations in the lift coefficient with time and therefore to high rms values. As an example let us focus on phase C. It is clear from the direction and angle of impingement of the flow stream that the lift coefficient will be positive–negative–positive for the cylinders 4, 5 and 6, respectively. This is confirmed by looking at Fig. 11(d)–(f). Similar conclusion about the signs of the lift coefficients can be obtained by scrutinizing the other phases and cylinders and checking with the actual values in Fig. 11. In a single cylinder the variation of lift and drag are associated with the unsteady wake behind it. For multiple cylinder configurations, however, the interaction of the wakes must be examined in order to explain the observed behaviour of the forces in one period.

The pressure distribution around each cylinder for the same four time instances is shown in Fig. 13. This pattern can be correlated with the corresponding streamlines in the previous figure. The high pressures at the impingement points but also the low pressures (due to Bernoulli effect) in the areas around the periphery where the flow stream accelerates are clearly visible. Note that these features have an additive effect on the lift. In order to see this let us focus again on phase C and in particular the fourth cylinder. Both the jet impingement from below and the low pressure due to flow acceleration at the top lead to high positive C_l value. Beyond the end of the array, strong negative pressure regions clearly demarcate the vortices shed by the last cylinder. It is interesting to see that the distance between those vortices behind the array is equal to the tube spacing, i.e. the vortices that are in phase are a distance $2s$ apart.

The vortex shedding pattern in phase B is shown in Fig. 14(a). Similar patterns are observed for the other phases as well. The 180° phase difference between successive rows (after the third cylinder) is clearly visualised. The overlapping of the vortex centers and the low pressure regions from the previous Fig. 13(b) is also evident.

For the shedding pattern described in the previous paragraphs to take place, the distance traveled by a vortex within one period should be equal to twice the distance between the tubes. This means that the time period is given by

$$T = \frac{2S_L}{U_c} = \frac{2sd}{U_c} \tag{3}$$

where U_c is the vortex convection velocity (also known as vortex celerity). From this equation the Strouhal number can be evaluated as

$$St = \frac{d}{TU_\infty} = \frac{U_c}{U_\infty}\frac{1}{2s} \tag{4}$$

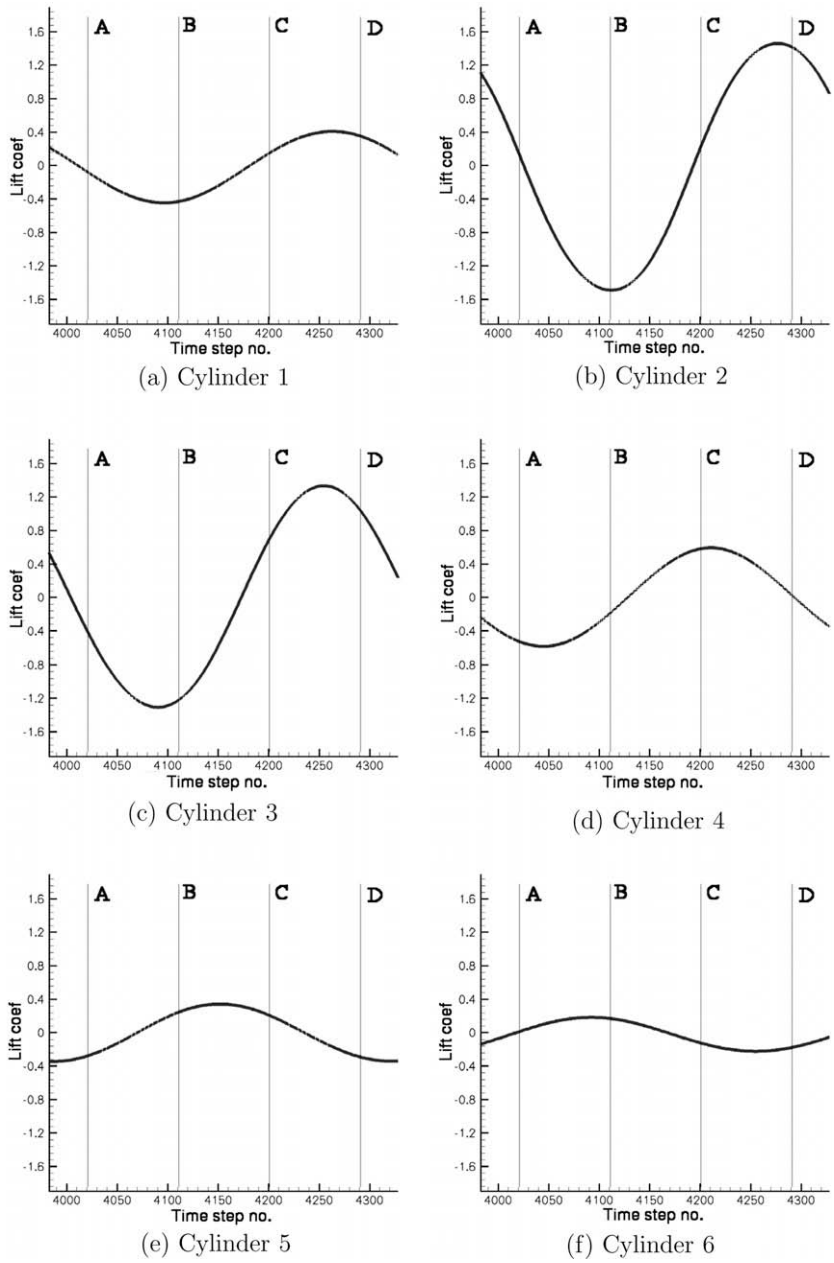

Fig. 15. Variation of the instantaneous lift coefficient with time and definition of phases A–D ($s = 4$).

For the flow around a single cylinder the vortex celerity has been studied by many investigators. Data from various sources were compiled by [10]. They found that for low Reynolds numbers (300, 360) the vortex celerity in the wake depends on the distance from the cylinder; it is smaller in the near field and larger in the far field. In the far field, all the studies examined show a value of $0.8U_\infty$ irrespective of the Reynolds number. A similar value ($0.78U_\infty$) is reported by [18] for $Re \approx 21{,}400$ for a rectangular cylinder. It was not possible to find in the literature values of convection velocity for tube bundles. However, this can be easily estimated by identifying one vortex and then tracing its location in the different phases. This was carried out for phases A–D and the vortex celerity was found to be the same between two successive phases and equal to around $0.8U_\infty$. It is interesting to see that this agrees with the aforementioned value for a single cylinder in the far field. Using this value in the previous Eq. (4) and substituting $s = 3.6$ we find that the predicted Strouhal number is equal to 0.111. This value is very close (difference less than 2%) to the one calculated numerically by Fourier transform and reported in Table 1.

Let us now turn our attention to $s = 4$. The variation in the lift coefficient is shown in Fig. 15. There is a phase difference between the signals in rows 4–6 but it is much smaller compared to the previous spacing. This is reflected in the instantaneous flow patterns shown in Fig. 16. It can now be seen that because of the increased spacing between the cylinders, the fluid stream has the available space to make a U-turn within the gaps due to the action of the vortices. This means that in most time instances the flow passes from the same side of two successive cylinders (for example from the top for cylinders 3 and 4 in phase C or from the bottom in phase A). In other instances, for example in phases B and D, the flow passes alternatively from opposite sides. The fact that the flow has the space to make a U-turn reduces significantly the phase

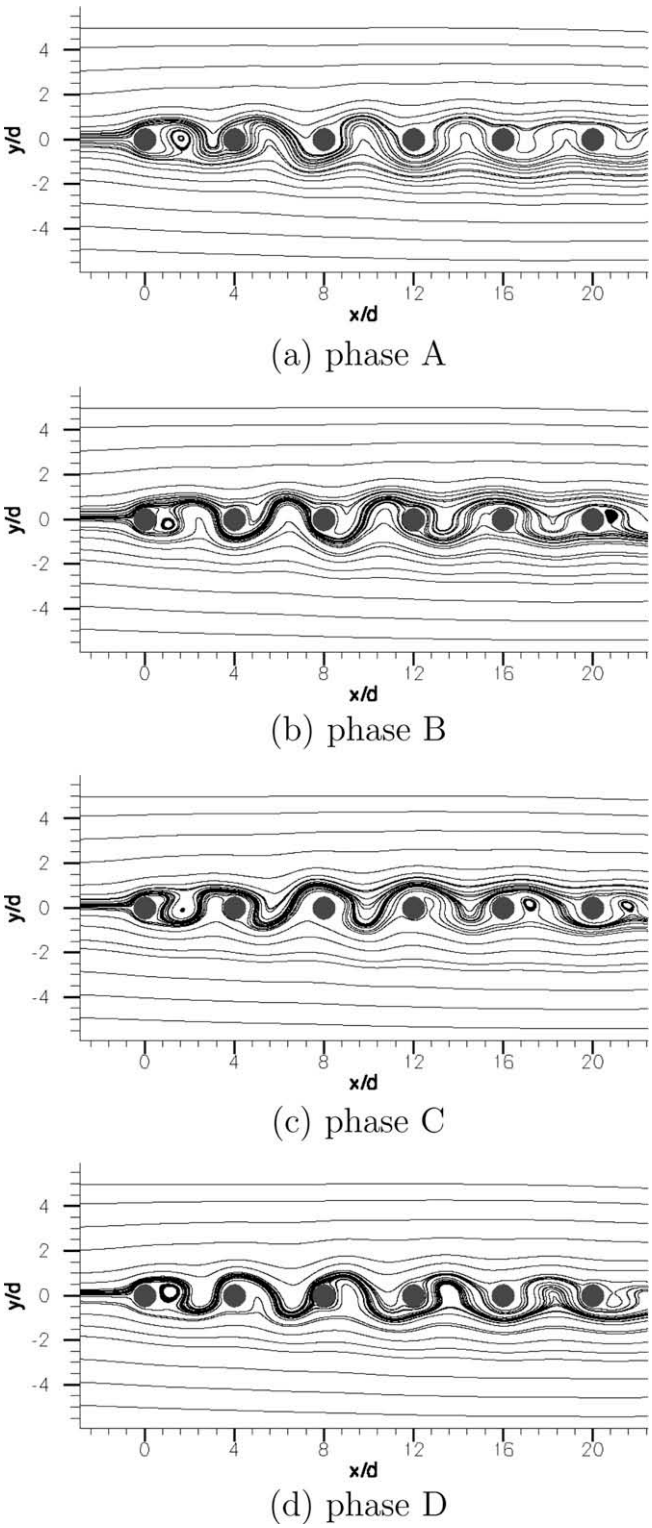

Fig. 16. Streamlines at phases A–D ($s = 4$).

difference as the local approaching flow is the same for two successive cylinders.

The vortex shedding pattern is shown in Fig. 14(b). The same minimum and maximum values are used in order to be able to compare the vortex strength between the two spacings, 3.6 and 4. The comparison clearly indicates a reduced vortex strength and therefore reduced pressure variations and rms lift are expected. It is believed that the reduced vortex strength is due to the lack of velocity acceleration around cylinders. For this arrangement, the distance between two cylinders is large and the vortex motions are no longer synchronised with the spacing. This results in a significant change in the Strouhal number. For this spacing it is significantly increased as shown in Table 1 and it approaches the value of a single cylinder (equal to 0.165).

5. Conclusions

This paper studies the effect of tube spacing on the flow characteristics for a six-row inline tube bank under laminar flow conditions. The numerical method is first validated for laminar flow past two-in-tandem cylinders and the predicted force statistics is in excellent agreement with the results of Sharman et al. [27]. Following the validation study, the flow in a tube array consisting of six cylinders at various spacings in tandem is examined. Increase of the spacing makes the flow more asymmetric and induces vortex shedding starting from the last cylinder and proceeding upstream. It was found that for the last three cylinders the force statistics are maximised in the spacing region 3.0–3.6 and then drop rapidly at $s = 4$. The instantaneous flow patterns for $s = 3.6$ reveal an antisymmetric vortex shedding activity, i.e. there is 180° phase difference from one cylinder to the next and during one period the vortices travel a distance twice the tube spacing. For $s = 4$, the vortices become much weaker, the strong antisymmetry disappears, and the vortex motion is no longer synchronised with the spacing leading to reduced rms forces.

Acknowledgement

The first author is grateful to the British Heart Foundation (Project Grant No. PG/06/029/20577) for funding his post-doctorial work during 2006–2007 at the University of Glasgow, UK.

References

[1] Arie H, Kiya M, Moriya M, Mori H. Pressure fluctuations on the surface of two circular cylinders in tandem arrangement. ASME J Fluids Eng 1983;105:161–7.
[2] Balabani S, Yianneskis M. An experimental study of the mean flow and turbulence structure of cross-flow over tube bundles. Proc IMechE C: J Mech Eng Sci 1996;210:317–31.
[3] Balabani S, Yianneskis M. Vortex shedding and turbulence scales in staggered tube bundle flows. Can J Chem Eng 1997;75(5):823–31.
[4] Beaudan P, Moin P. Numerical experiments on the flow past a circular cylinder at a subcritical Reynolds number, Tech. Rep. TF-62, Thermosciences Division, Department of Mechanical Engineering, Stanford University; 1994.
[5] Hassan YA, Ibrahim WA. Turbulence prediction in two-dimensional bundle flows using large eddy simulation. Nucl Technol J 1997;119:11–28.
[6] Huang Z, Olson JA, Kerekes RJ, Green SI. Numerical simulation of the flow around rows of cylinders. Comput Fluids 2006;35:485–91.
[7] Igarashi T, Suzuki K. Characteristics of the flow around three circular cylinders arranged in-line. JSME 1984;27:2397–404.
[8] Issa RI. Solution of the implicitly discretized fluid flow equations by operator splitting. J Comput Phys 1986;62:40–65.
[9] Jester W, Kallinderis Y. Numerical study of incompressible flow about fixed cylinder pairs. J Fluids Struct 2003;17:561–77.
[10] Kim W, Yoo J, Sung J. Dynamics of vortex lock-on in a perturbed cylinder wake. Phys Fluids 2006;18:074103.
[11] Konstantinidis E, Castiglia D, Balabani S, Yianneskis M. On the flow and vortex shedding characteristics of an inline tube bundle in steady and pulsating cross-flow. Trans IChemE A: Chem Eng Res Design 2000;78(8):1129–38.
[12] Lam K, Cheung W. Phenomena of vortex shedding and flow interference of three cylinders in different equilateral arrangements. J Fluid Mech 1988;196:1–26.
[13] Lam K, Fang X. The effect of interference of four equispaced cylinders in cross flow on pressure and force coefficients. J Fluids Struct 1995;9:195–274.
[14] Lam K, Li J, So R. Force measurements and Strouhal numbers of four cylinders in cross flow. J Fluids Struct 2003;18:305–24.
[15] Li T, Deen NG, Kuipers JAM. Numerical investigation of hydrodynamics and mass transfer for in-line fiber arrays in laminar cross-flow at low reynolds numbers. Chem Eng Sci 2005;60:1837–47.
[16] Liang C, Papadakis G. Large eddy simulation of flow over a staggered tube bundle at subcritical Reynolds number. J Fluids Struct 2007;23:1215–30.
[17] Liang C, Papadakis G. Large eddy simulation of pulsating flow over a circular cylinder at subcritical Reynolds number. Comput Fluids 2007;36:299–312.

[18] Lyn D, Einav S, Rodi W, Park J. A laser-doppler velocimetry study of ensemble-averaged characteristics of the turbulent near wake of a square cylinder. J. Fluid Mech 1995;304:285–319.
[19] Mittal S, Kumar V, Raghuvanshi A. Unsteady incompressible flows past two cylinders in tandem and staggered arrangements. Int J Numer Meth Fluids 1997;25:1315–44.
[20] Oengören A, Ziada S. An in-depth study of vortex shedding, acoustic resonance and turbulent forces in normal triangle tube arrays. J Fluids Struct 1998;12:717–58.
[21] Owen P. Buffeting excitation of boiler tube vibration. J Mech Eng Sci 1965;7:431–9.
[22] Papaioannou GV, Yue D, Triantafyllou M, Karniadakis GE. Three-dimensionality effects in flow around two tandem cylinders. J Fluid Mech 2006;558:387–413.
[23] Patil R, Bharti R, Chhabra R. Steady flow of power law fluids over a pair of cylinders in tandem arrangement. Ind Eng Chem Res 2008;47:1660–83.
[24] Polak DR, Weaver DS. Vortex shedding in normal triangular tube arrays. J Fluids Struct 1995;9:1–17.
[25] Price JS, Païdoussis MP, Mark B. Flow visulisation of the interstitial cross-flow through parallel triangular and rotated square arrays of cylinders. J Sound Vibr 1995;181:85–98.
[26] Rhie CM, Chow WL. Numerical study of the turbulent flow past an airfoil with trailing edge separation. AIAA J 1983;21:1525–32.
[27] Sharman B, Lien FS, Davidson L, Norberg C. Numerical predictions of low Reynolds number flows over two tandem circular cylinders. Int J Numer Meth Fluids 2005;47:423–47.
[28] Simonin O, Barcouda M. Measurements and prediction of turbulent flow entering a staggered tube bundle. In: Proceedings of fourth international symposium on applications of laser anemometry to fluid mechanics, Lisbon, paper number 5.23; 1988.
[29] Sumner D, Price SJ, Païdoussis MP. Flow-pattern identification for 2 staggered circular cylinders in cross-flow. J Fluid Mech 2000;411:263–303.
[30] Sumner D, Richards MD, Akosile OO. Two staggered circular cylinders of equal diameter in cross-flow. J Fluids Struct 2005;20:255–76.
[31] Weaver D, Fitzpatrick J, El Kashlan M. Strouhal numbers for heat exchanger tube arrays in cross flow. J Press Vessel Technol 1987;109:219–23.
[32] Weaver DS, Lian HY, Huang XY. Vortex shedding in rotated square arrays. J Fluids Struct 1993;7:107–21.
[33] Zdravkovich MM. Review of flow interference between two circular cylinders in various arrangements. ASME J Fluids Eng 1977;99:618–33.
[34] Ziada S, Oengören A. Vorticity shedding and acoustic resonance in an inline tube bundle. Part I: vorticity shedding. J Fluids Struct 1992;6:271–92.
[35] Ziada S, Oengören A. Vortex shedding in an inline tube bundle with large tube spacings. J Fluids Struct 1993;7:661–87.
[36] Ziada S, Oengören A. Flow periodicity and acoustic resonance in parallel triangle tube bundles. J Fluids Struct 2000;14:197–219.